Tailoring the Mechanical Properties of High-Aspect-Ratio Carbon Nanotube Arrays using Amorphous Silicon Carbide Coatings

*René H. Poelma, Bruno Morana, Sten Vollebregt, Erik Schlangen, Henk W. van Zeijl, Xuejun Fan, and Guo Qi Zhang**

The porous nature of carbon nanotube (CNT) arrays allows for the unique opportunity to tailor their mechanical response by the infiltration and deposition of nanoscale conformal coatings. Here, we fabricate novel photo-lithographically defined CNT pillars that are conformally coated with amorphous silicon carbide (a-SiC) to strengthen the interlocking of individual CNTs at junctions using low pressure chemical vapor deposition (LPCVD). We further quantify the mechanical response by performing flat-punch nanoindentation measurements on coated CNT pillars with various high-aspect-ratios. We discovered new mechanical failure modes of coated CNT pillars, such as "bamboo" and brittle-like composite rupture as coating thickness increases. Furthermore, a significant increase in strength and modulus is achieved. For CNT pillars with high aspect ratio (1:10) and coating thickness of 21.4 nm, the compressive strength increases by an order of magnitude of 3, towards 1.8 GPa (from below 1 MPa for uncoated CNT pillars) and the elastic modulus increases towards 125 GPa. These results show that our coated CNT pillars, which can serve as vertical interconnects and 3D super-capacitors, can be transformed into robust high-aspect-ratio 3D-micro architectures with semiconductor device compatible processes.

1. Introduction

Vertically aligned carbon nanotube (CNT) arrays or forests in photo-lithographically defined patterns have been recognized as a promising structural material for the fabrication of high-aspect-ratio, three-dimensional (3D) micro- and nano-architectures.[1–5] The exceptional properties of CNTs and related materials have triggered tremendous efforts not only to study their intrinsic properties but also to explore their applications in a large variety of fields.[6–13] These high-aspect-ratio 3D structures play an important role in the advancement of vertical interconnect technology,[14–17] flexible batteries,[3] stamps for micro/nanoimprint lithography,[2,18–21] compliant thermal interface materials for low inter-facial resistances,[22–25] 3D super-capacitors[26,27] and nano/micro-electromechanical systems (NEMS) and (MEMS).[1,28–30]

The CNT arrays that we refer to in this work are composed of nominally vertical, interwoven, multi-wall carbon nanotubes.[31,32] A common procedure for growing high-aspect-ratio CNT arrays is via chemical vapor deposition (CVD) on photo-lithographically defined catalyst areas.[5,9] One of the limitation of this growth process, is the low packing density of the CNTs inside the array.[15,33] The interwoven CNTs inside the array are held together by a weak van der Waals interaction, allowing tubes to slide along each other.[34,35] The combination of low packing density and weak inter-tube forces, results in mechanical properties of CNT arrays that are significantly inferior to individual CNTs.[6,35]

Consequently, a considerable amount of effort is going into the development of new methods to optimize the full potential of individual CNTs in low density CNT arrays, either by densification or application of conformal coatings. A literature overview of coated nanoscale architectures discusses the inherent link between nanoscale morphology and properties.[36] Recent and remarkable examples of conformally coated CNT arrays include e.g., deposition of silicon coatings to create a flexible anode architecture for high-energy-density-batteries[3] and graphene coatings to create superelastic, lightweight and fatigue resistant aerogels.[7]

Silicon carbide (SiC) also proves to be an interesting coating material, mainly due to its diamond like characteristics.[37] The properties of SiC are especially attractive in applications which require contact, high temperatures, chemical inertness, high robustness, electrical conductivity and high resistance to

R. H. Poelma, B. Morana, S. Vollebregt, Dr. H. W. van Zeijl, Prof. G. Q. Zhang
Department of Microelectronics
Delft University of Technology
Feldmannweg 17
2628CT, Delft, The Netherlands
E-mail: G.Q.Zhang@tudelft.nl
Prof. E. Schlangen
Department of Structural Engineering
Delft University of Technology
Stevinweg 1
2628CN, Delft, The Netherlands
Prof. X. J. Fan
Department of Mechanical Engineering
Lamar University
Beaumont, TX 77710, USA

DOI: 10.1002/adfm.201400693

electron beam damage.[38–41] Bulk composites containing SiC-coated CNTs have been produced by chemical vapor infiltration and were tested by bending and a pull-out method. One remarkable result was the protection of CNTs from being oxidized at 1600 °C in air for 1 hour.[42] Investigations have also shown that SiC-coated multi-walled CNTs dispersed in composites increase fracture toughness and hardness.[43]

The porosity of CNT arrays allows for infiltration and deposition of conformal coatings on individual CNTs inside the array. This results in the possibility to significantly alter the mechanical response of 3D-micro-architectures by changing the deposition thickness.

In this paper, we report the fabrication and testing of various high-aspect ratio pillars made from carbon nanotube arrays that are modified by thin conformal coatings of amorphous silicon carbide (a-SiC) deposited by low pressure chemical vapor deposition. We perform flat-punch nanoindentation measurements on CNT pillars to characterize the influence of conformal coatings of different thickness on the mechanical response of 3D-micro-architectures. We analyze the structural failure mode by performing scanning electron microscopy investigations after pillar compression. The specimens without coating show localized periodic buckling. Samples with thin coatings show bamboo-like failure while the samples with thick coatings show brittle ceramic failure. Furthermore, a significant increase of 3 orders of magnitude is measured for the compressive strength of pillars with a 21.4 nm thick coating of a-SiC.

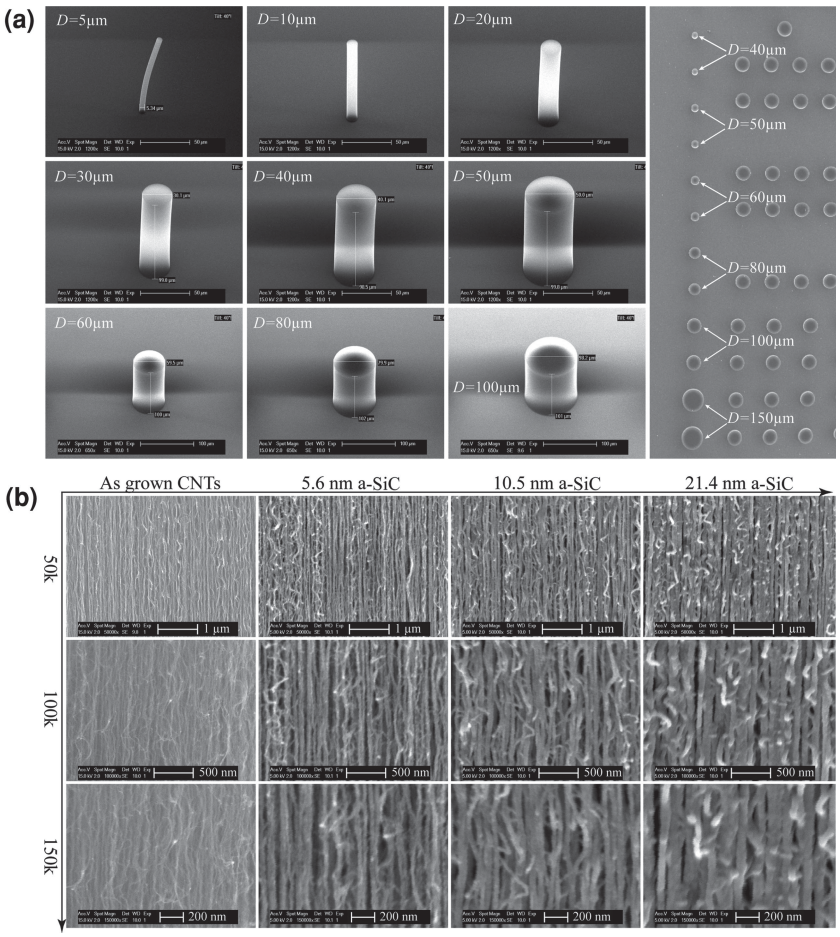

Figure 1. Scanning electron microscopy images of a) CNT pillars with varying aspect ratios on the left tilted views, on the right top view. b) The morphology of the CNT pillar sidewall before and after a-SiC deposition at different magnifications.

2. Results and Discussion

Carbon nanotube structures are grown by a common manufacturing process employing CVD on photo-lithographically defined catalyst areas (Section S1, Supporting Information). After growth, the CNT arrays are conformally coated with 5.6 nm, 10.5 nm, 21.4 nm and 52.0 nm thin layers of amorphous silicon carbide (a-SiC) (Section S2, Supporting Information).

A matrix of as-grown CNT pillars with circular cross sections is shown in **Figure 1**a. The pillars are (100 ± 2) µm tall and have lithographically defined diameters ranging from (5 ± 1) µm to (150 ± 1) µm. The maximum length to diameter L/D aspect ratio that results in highly vertical pillars is about 10:1. The morphology of the CNT pillars at 50, 100 and 150k magnification is shown in Figure 1b, here it can be seen that individual CNTs inside the array are nominally vertical and interwoven. The low packing density is mainly caused by the relatively large spacing between catalyst particles which results in large spacing between individual CNTs.[33] Examination of the CNT arrays at different stages; before and after coating, allows us to verify the coating process. Some single CNT fibers are bundled together into larger fibers due to the van der Waals attraction. The high magnification images in Figure 1b, show a doubling of the fiber thickness with increasing deposition thickness, following the same trend as the measured film thicknesses of 5.6 nm, 10.5 nm, 21.4 nm and 52.0 nm of a-SiC on bare Si test wafers (Figure S2, Supporting Information). The as-grown CNT array density is roughly 10^{10} tubes cm^{-2} which is determined from the SEM images of the pillars in Figure 1b. The samples with a thick coating are still somewhat porous, this shows that precursor gases can still infiltrate the array and deposit a-SiC further inside the bundle.

To investigate the coating penetration depth and thickness we cleave several coated micropillars with a Berkovich nanoindentation tip. Afterwards, we use a Verios 460 extreme-high-resolution (XHR) SEM for characterization of the pillar cross-section. The coating thickness reduces with roughly 0.14 nm per 1 µm surface penetration depth (Figure S3, Supporting Information). Closer inspection reveals that the CNTs, which are sticking out of the broken a-SiC matrix, have an average diameter of about 9 nm (Figure S4, Supporting Information). Furthermore, the high resolution SEM image shows that the

coating thickness on the CNTs is in excellent agreement with the film thickness measured by ellipsometry on flat control samples.

A Raman spectrum analysis of the pillars is used to assess the quality of the CNTs before and after a-SiC deposition. The data shows a convolution of the graphite (G) and disordered graphite (D) peaks together with the a-SiC peak into a single wide asymmetric peak near 1475 cm^{-1} (Figure S5, Supporting Information). Deconvolution of the peaks using a least square fitting procedure shows that the intensity ratio I_G/I_D is reduced for thicker films of a-SiC. This indicates that the deposition of a-SiC might have reduced the quality of the CNTs. However, the scattering efficiency of amorphous carbon is relatively high when compared to graphite like carbon. The amorphous carbon would therefore yield a stronger Raman signal, which originates more from surface layers instead of the CNTs.

2.1. Compressive Failure of Uncoated CNT Pillars

Uniaxial compression tests of micro- and nano-pillars using flat-punch nanoindentation offers a convenient method to effectively study their mechanical behavior with high accuracy and precision.[44] The mechanical response of our CNT pillars under uniaxial compression is characterized using nanoindentation with a custom-made flat-punch diamond indentation tip. The nanoindentation procedure is discussed in more detail in the Supporting Information and displayed in Figure S6. Scanning electron microscopy images of uncoated CNT pillars after compression reveal that the pillar failure mode is a type of localized periodic buckling which initiates at the base and propagates upwards throughout the entire bundle for increased compression depth, see **Figure 2**a. The top three pillars with 100 µm, 80 µm and 60 µm diameters were compressed 25%, 20% and 17% respectively and show 1 or 2 buckling-wavenumbers. The bottom three pillars with 50 µm, 40 µm and 30 µm diameters were compressed 80% and show wavenumbers in the range of 9 to 11. These typical buckling characteristics appear to be unique for uncoated CNT arrays. More importantly, the localized periodic buckling events are very reproducible and in excellent agreement with the in situ CNT array compression observations from Hutchens and Maschmann et al.[5,9] Their observations also indicate that buckling events originate at the base of the pillar and the buckling

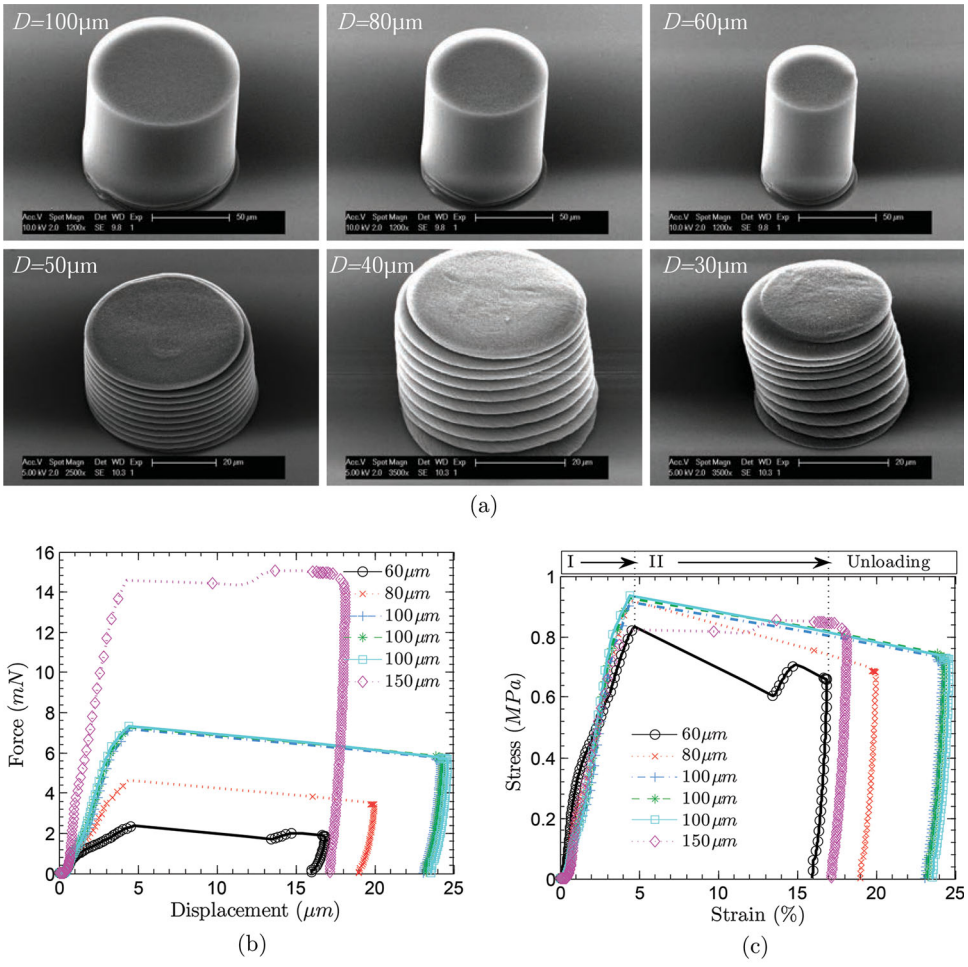

Figure 2. Mechanical response of uncoated CNT pillars. a) SEM images showing the compressive failure of uncoated CNT pillars of different diameters. The top row was compressed 20 µm, the smaller diameter pillars were compressed 80 µm. b) The measured load versus displacement and c) the engineering stress versus strain response.

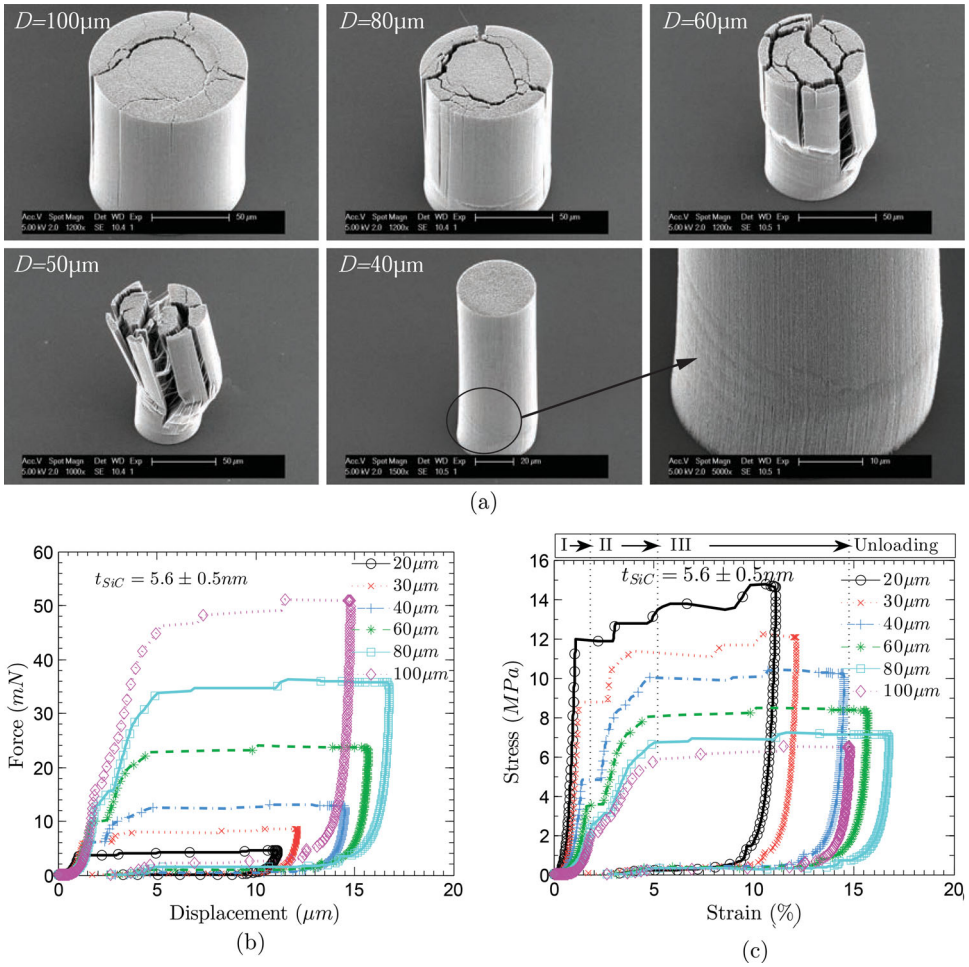

Figure 3. Mechanical response of CNT pillars with a 5.6 nm thick a-SiC coating. a) SEM images showing the compressive failure of coated CNT pillars of different diameters. b) The measured load versus displacement and (c) the engineering stress versus strain response.

wave-number increases with increasing compression depth of the pillars. The load-displacement and stress-strain response up until failure of uncoated CNT pillars are shown in Figure 2b and Figure 2c respectively. Multiple measurements on different pillars with a 100 µm diameter show a high degree of repeatability. Measurement on a 60 µm diameter pillar show that the stress increases monotonically for increasing compression, see regime (I) in Figure 2c. The maximum stress that can be applied before the pillar collapses is about 0.85 MPa at a critical compressive strain of about 4.8%. When this stress is exceeded the system transitions from a stable regime (I) towards an unstable regime (II) with rapid strain bursts. The large distance between the line markers indicates buckling or structural collapse of the pillar which results in an overshoot of the nanoindentation tip towards the substrate. The displacement control of the nanoindenter-equipment is not fast enough to capture the fast decrease in load when the specimen fails. In the final unloading regime it is shown that the pillars remain permanently deformed with little strain recovery $\varepsilon_r \leq 2\%$. The volume shrinkage after buckling is therefore about equal to the amount of compression and can be as high as 60% to 80% of the original volume, see Figure 2a. Uncoated pillars with diameters below 60 µm proved to be too challenging to measure due to adhesion of the pillars to the indentation tip and are therefore omitted from the results.

2.2. Compressive Failure of Coated CNT Pillars

An exciting observation can be made from the post compression morphology of pillars with a 5.6 nm thin conformal coating of a-SiC, see **Figure 3**a. We see highly aligned vertical cracks and barely visible wrinkles on the outer surface which have originated from localized buckling and kinking of the CNT fibers. Furthermore, the failure does not initiate from the base and the distinctive periodic buckling which appeared in uncoated pillars, is no longer observed.

The results indicate composite failure in the form of matrix or matrix - CNT interface failure. From a cylindrical perspective, vertical cracks are induced when the circumferential stress at the exterior of the pillar exceeds the composite strength. Circumferential stress is strongly dependent on radius and internal pressure. During compression, the pillar internal pressure might increase due to internal localized periodic buckling events that exert pressure on the surrounding material. As a consequence, a strong diameter dependency is observed in the compressive

strength of the coated pillars. The mechanism is then crack propagation inside the matrix parallel to the fiber (CNT) orientation. This leads to gradual crushing and a distinct splitting shape of failed pillars resembling bamboo under uniaxial compressive loads.[45,46]

When compared to the uncoated CNT pillars, the mechanical behavior changed from a foam-like material, where the dominant failure mode is localized periodic buckling, towards a bamboo-like failure similar to typical fiber reinforced composites. The accompanying stress versus strain response of the coated pillars see Figure 3c, show an increase in compressive strength and a strong diameter dependency, where the small 20 µm diameter pillars have higher compressive strengths of about 12 MPa. Three distinct regimes can be identified; regime (I) ($0\% \leq \varepsilon \leq 2\%$) elastic deformation, regime (II) ($2\% \leq \varepsilon \leq 5\%$) small strain burst propagation, while regime (III) ($\varepsilon > 5\%$) shows large strain burst propagation. The regimes (I), (II) and (III) have been illustrated in Figure 3c for a 100 µm diameter pillar. The compressive strength of the pillars is defined as the maximum stress that can be applied before transition occurs from regime (I) to (II). We think that regime (II) can be attributed to non-periodic local buckling while regime (III) is composite failure and splitting of the bundle.

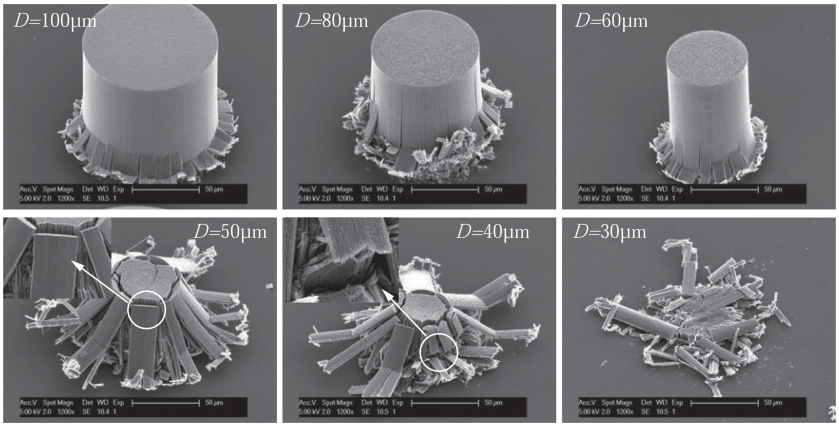

Figure 4. Compressive failure of CNT pillars coated with 10.5 nm a-SiC.

Furthermore, a significant recovery of 70% for all deformed pillars towards their original position occurs during unloading even though cracks have appeared. The attraction between CNTs becomes more prominent as they come in closer proximity during compression, which can result in sticking and therefore low recovery of uncoated CNT arrays.[47] This suggests that during compression of coated CNTs with 5.6 nm a-SiC, the elastic energy stored inside the coated CNTs is enough to overcome the attractive van der Waals force. At the same time the coating is thin enough to allow for a certain degree of flexibility before fracturing. Moreover, the coating interlocks and constrains most of the interwoven CNTs at their junctions. Thus, preventing the tubes from sliding and rotating along each other by replacing the relatively weak van der Waals interaction with a solid cohesive bond and therefore preventing energy dissipation. We hypothesize that these effects combined, attribute to an improved strain recovery of the coated CNT array.

Post compression inspection of samples with thicker coatings of 10.5 nm and 21.4 nm of a-SiC, reveal a more destructive failure, see **Figure 4** and **Figure 5** respectively. This can be related to a more dominant brittle failure mode of the a-SiC matrix when the coating thickness is increased. Furthermore, a type of kink banding failure is initiated at the base of the pillar at a similar location as the localized buckling events in uncoated samples. In addition, CNT fibre fracture is observed after compressive failure. The stress strain curves **Figure 6**b and Figure 6d confirm brittle failure due to the almost instantaneous transition from the elastic regime towards structural collapse without yielding, strain bursts or localized buckling events. Finally we tested samples with a coating thickness of 52.0 nm of a-SiC. The pillars were too strong and could not be damaged due to the maximum load limitations of the nanoindentation equipment, see Figure 6e and Figure 6f. With the use of a Berkovich tip the pillars were finally destroyed, see Figure S8. Due to the very strong pillar and violent destruction, the fracture propagated from the pillar into the bulk Si substrate.

The compressive strength of CNT pillars with different coating thickness has been examined. Their strength is defined as the maximum stress that can be applied before initiation of strain bursts, buckling or structural collapse occurs. This corresponds with the transition of regime (I) towards regime (II). **Figure 7** displays an overview of the maximum compressive stress of high-aspect ratio coated and uncoated CNT pillars. A high degree of repeatability is found for measurements on different pillars with a 100 µm diameter, each average is composed of about 12 measurements. For the smaller diameter pillars the average is composed of 1 to 4 measurements, since these pillars are fewer in number. The compressive stress increases with thicker coatings and for decreasing pillar diameter. A relatively high compressive strength (800 MPa to 1.8 GPa) is achieved for high-aspect ratio pillars ($L/D > 100{:}30$) with 21.4 nm thick coatings of a-SiC. The significant increase in compressive

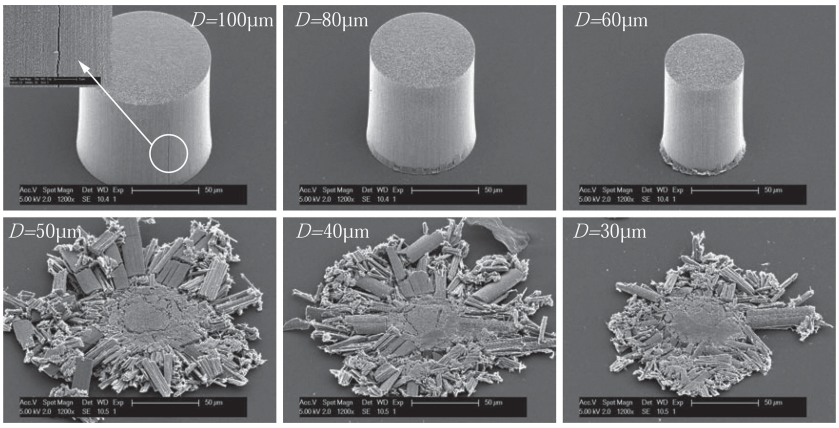

Figure 5. Compressive failure of CNT pillars coated with 21.4 nm a-SiC.

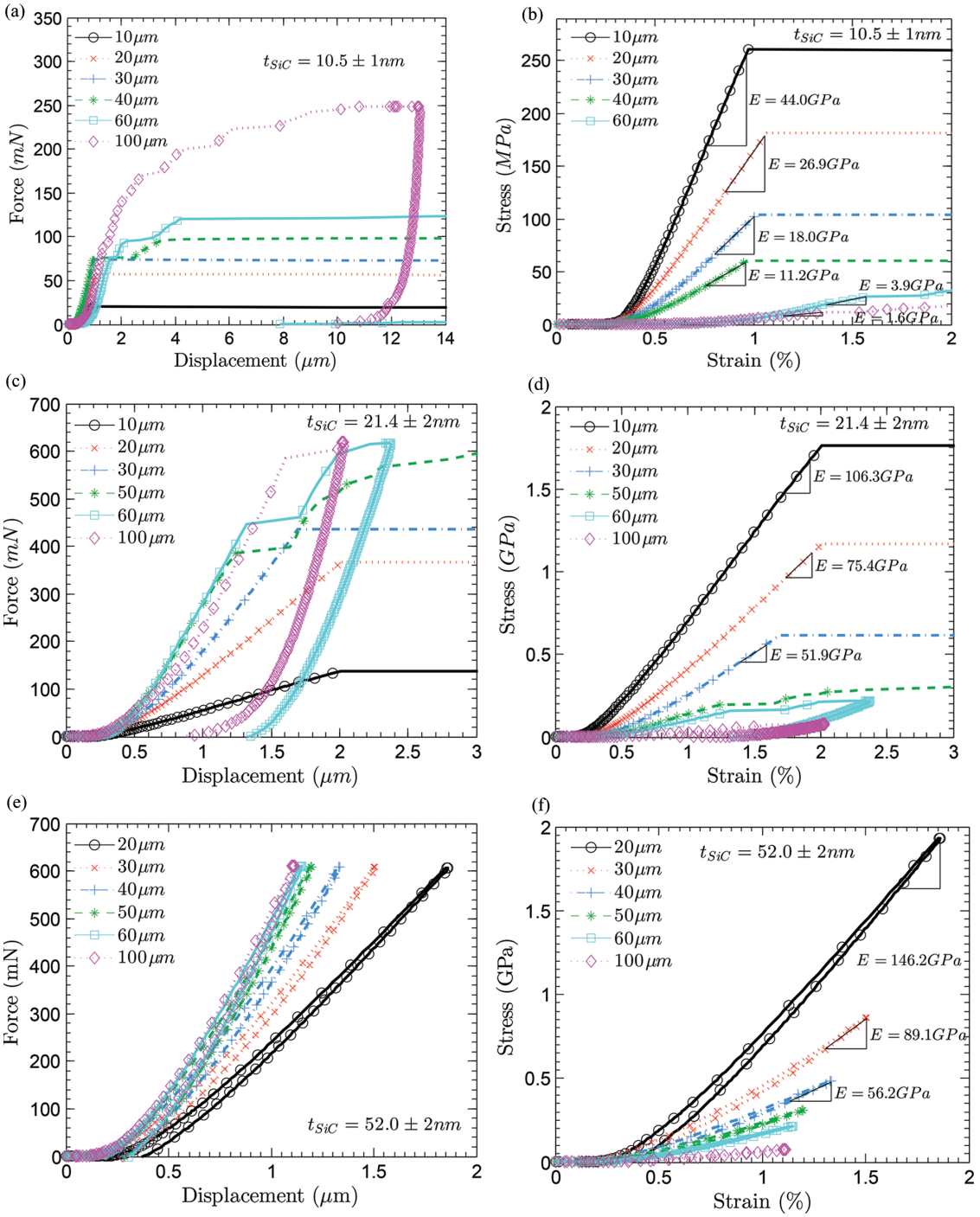

Figure 6. Mechanical response of CNT pillars with a 10.5 nm, 21.4 nm and a 52.0 nm thick a-SiC coating. a,c,e: The measured load versus displacement and b,d,f: the engineering stress versus strain response.

stress is about 3 orders of magnitude higher than uncoated pillars. It shows that careful control of nanometer thin conformal coatings of a-SiC can increase the strength of CNT array microstructures by several orders of magnitude.

For the uncoated pillars, owing to the low density and waviness of the long and slender CNTs inside the array, it is expected that they mostly carry bending and torsional forces instead of normal forces. This draws a strong resemblance with open-cell foams.[48,49] When a conformal coating of 21.4 nm is applied to the CNTs, the porosity of the array is reduced from roughly 99% to 79% (Supplementary S3) and the bending stiffness of the highly flexible CNTs inside the pillar is increased. Moreover, the contribution from normal forces or stiffness originating from CNT fiber extension and compression becomes more significant as coating thickness increases. The coating interlocks and constrains the interwoven CNTs

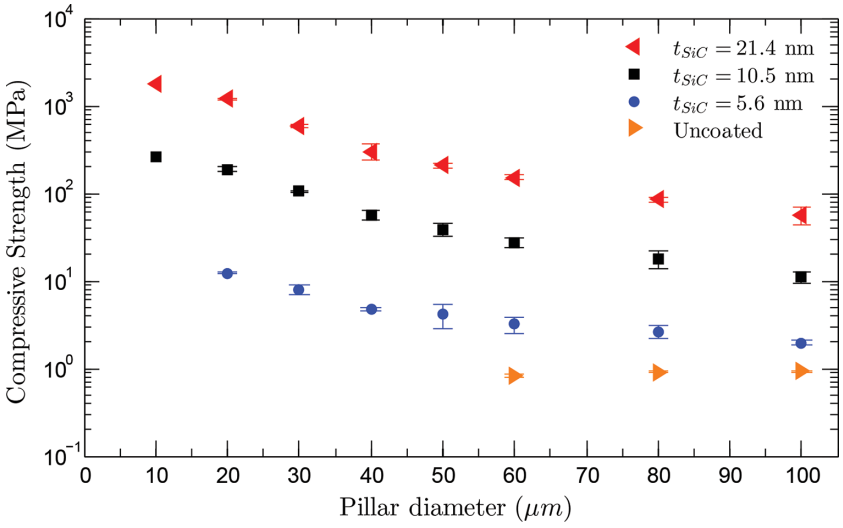

Figure 7. Compressive failure stress of coated and uncoated pillars.

at their junctions. With a thicker coating, a larger distance between the CNTs can be bridged, subsequently bonding more CNTs together and reducing the porosity. As a consequence, the mechanical response of coated CNT arrays changes from foam-like, towards bamboo-like and finally brittle-ceramic-like as coating thickness increases. A coating thickness gradient will cause the effective mechanical material properties of the pillar to strongly increase in radial direction from the center. Thus, explaining the diameter dependency of the material properties of the coated pillars and drawing additional similarities with other types of orthotropic materials such as wood or bamboo.

2.3. Young's Modulus

The effects of thin conformal a-SiC coatings on *E* the Young's modulus of CNT pillars are measured using the continues stiffness measurement (CSM) mode of the nanoindenter (Supporting Information S5). The uncoated samples and those with a thin a-SiC coating of 5.6 nm have all collapsed before a plateau region was reached (Figure S7a and Figure S7b, Supporting Information). The effective Young's modulus of coated pillars increases drastically with increasing coating thickness. We find that the Young's modulus increases with compression depth and plateau regions are observed for samples with 10.5 and 21.4 nm thick a-SiC coatings. The measured moduli in Figure S7, Supporting Information, are in excellent agreement with the moduli extracted from the slope of the stress-strain curves before failure occurs, see Figure 6b and Figure 6d, respectively. Another observation shows that *E* increases for coated pillars of smaller diameter, following the same trend as the compressive strength Figure 7. A gradient in the coating thickness as a function of the surface penetration depth can be a possible explanation for the observed pillar diameter dependency of the compressive strength and Young's modulus measurements, (Supporting Information S2) gives a more in depth analysis.

3. Conclusions

Carbon nanotube pillars were grown and their mechanical response was modified from foam like towards brittle ceramic behavior, using a straightforward process of depositing nanoscale conformal coatings of amorphous silicon carbide (a-SiC) by low pressure chemical vapor deposition. The failure mode of coated pillars was characterized using nanoindentation with a flat cylindrical punch. The dominant failure mode changed from localized periodic buckling towards bamboo-like failure and finally towards brittle ceramic failure as coating thickness increased. Vertical cracks at the exterior of the pillar were induced when the circumferential stress exceeded the composite strength during compression. We conclude that conformal coatings reduce the porosity of the array and increase the stiffness of the highly flexible CNTs. Furthermore, the connections between neighboring tubes inside the CNT array are increased and changed from weak van der Waals interaction for the uncoated arrays, towards a bonded a-SiC connection.

As a result, a tremendous increase of 3 orders of magnitude for the Young's modulus and compressive strength of pillars with a 21.4 nm thick deposition of a-SiC was achieved. The Young's moduli increased from 200 MPa for uncoated pillars at 1 µm compression depth towards a high value of about 125 GPa for a 10 µm diameter pillar with a thin conformal coating of 21.4 nm a-SiC. Furthermore the compressive strength of uncoated pillars increased from values below 1 MPa towards a maximum of 1.8 GPa. We therefore propose that the fast growing, conformal coated, CNT arrays can be useful as a strong structural material for creating robust high aspect ratio 3D-micro architectures.

4. Experimental Section

CNT Growth: The first step in the synthesis of different aspect-ratio CNT pillars consists of growing a 170 nm thick thermal silicon oxide layer on a silicon wafer substrate to prevent diffusion of the metal catalyst into the substrate. Next, a 15 nm thin layer of alumina (Al_2O_3) is sputtered on the substrate to increase the CNT nucleation density from the catalyst particles.[50] For the lift-off process we spin coat and pattern, using optical lithography, a film of 1.5 µm thick negative photoresist (AZ Nlof2000). Then a 2 nm thin layer of iron (Fe) catalyst is deposited on the Al_2O_3 film by electron beam evaporation. The catalyst is patterned by a lift-off process using a NMP (C_5H_9NO) solvent at 70 °C for dissolving the resist. Next, (100 ± 2) µm tall vertically aligned multi-wall CNTs are grown in 5 minutes by low pressure chemical vapor deposition (LPCVD) in a commercial deposition system (Black Magic Pro, Aixtron). The CNTs are grown at a temperature of 600 °C using a gas flow mixture of 700 sccm hydrogen over 50 sccm acetylene (H_2/C_2H_2) at 80 mbar.

Conformal Coating: The a-SiC films are deposited inside a Tempress hot-wall LPCVD furnace using dichlorosilane (SiH_2Cl_2) and acetylene (C_2H_2) as gas precursor diluted at 5% in hydrogen (H_2). The deposition temperature and pressure are set to 760 °C and 1 mbar, respectively. The gas flow rates are 65 sccm SiH_2Cl_2 over 435 sccm C_2H_2 in 5% H_2. A

detailed description of different SiC deposition process recipes and their characterization is described in previous work.[38]

Mechanical Characterization: The mechanical response of CNT pillars is characterized using nanoindentation with an Agilent MTS Nanoindenter XP G200. Uniaxial compression of the CNT pillars was achieved by using a 150 μm diameter custom made flat-punch diamond indenter tip. For each test we detect the surface on a neighboring pillar to avoid affecting the pillar on which measurements are performed. Force, displacement and stiffness data were acquired using the continuous stiffness measurement (CSM) technique. The CSM settings used are: 2 nm amplitude, 45 Hz frequency, sensitive 100 N m^{-1} surface detection and a strain rate of 0.01 s^{-1}.

Supporting Information

Supporting Information is available from the Wiley Online Library or from the author.

Acknowledgements

We wish to acknowledge the support of the DIMES Technology Centre for their assistance during the clean room processing, I.G.C. Weppelman and C.Th.H. Heerkens from the Charged Particle Optics group for the Verios 460 extreme-high-resolution (XHR) SEM support.

Received: March 1, 2014
Revised: April 3, 2014
Published online: July 17, 2014

[1] Y. Hayamizu, T. Yamada, K. Mizuno, R. C. Davis, D. N. Futaba, M. Yumura, K. Hata, *Nat. Nanotechnol.* **2008**, *3*, 289.
[2] M. De Volder, S. H. Tawfick, S. J. Park, D. Copic, Z. Zhao, W. Lu, A. J. Hart, *Adv. Mater.* **2010**, *22*, 4384.
[3] K. Fu, O. Yildiz, H. Bhanushali, Y. Wang, K. Stano, L. Xue, X. Zhang, P. D. Bradford, *Adv. Mater.* **2013**, *25*, 5109.
[4] S. Tawfick, M. De Volder, A. J. Hart, *Langmuir* **2011**, *27*, 6389.
[5] S. B. Hutchens, L. J. Hall, J. R. Greer, *Adv. Funct. Mater.* **2010**, *20*, 2338.
[6] M. F. L. De Volder, S. H. Tawfick, R. H. Baughman, A. J. Hart, *Science* **2013**, *339*, 535.
[7] K. H. Kim, Y. Oh, M. F. Islam, *Nat. Nanotechnol.* **2012**, *7*, 562.
[8] Q. Tang, Z. Zhou, Z. Chen, *Nanoscale* **2013**, *5*, 4541.
[9] M. R. Maschmann, G. J. Ehlert, S. J. Park, D. Mollenhauer, B. Maruyama, A. J. Hart, J. W. Baur, *Adv. Funct. Mater.* **2012**, *22*, 4686.
[10] V. P. Veedu, A. Cao, X. Li, K. Ma, C. Soldano, S. Kar, P. M. Ajayan, M. N. Ghasemi-Nejhad, *Nat. Mater.* **2006**, *5*, 457.
[11] A. Cao, P. L. Dickrell, W. G. Sawyer, M. N. Ghasemi-Nejhad, P. M. Ajayan, *Science* **2005**, *310*, 1307.
[12] A. Cao, V. P. Veedu, X. Li, Z. Yao, M. N. Ghasemi-Nejhad, P. M. Ajayan, *Nat. Mater.* **2005**, *4*, 540.
[13] P. D. Bradford, X. Wang, H. Zhao, Y. T. Zhu, *Carbon* **2011**, *49*, 2834.
[14] S. Vollebregt, F. D. Tichelaar, H. Schellevis, C. I. M. Beenakker, R. Ishihara, *Carbon* **2014**, *71*, 249.
[15] L. Zhengchun, L. Ci, S. Kar, P. M. Ajayan, L. Jian-Qiang, *IEEE Trans. Nanotechnol.* **2009**, *8*, 196.
[16] A. Naeemi, J. D. Meindl, *Ann. Rev. Mater. Res.* **2009**, *39*, 255.
[17] Y.-C. Tseng, P. Xuan, A. Javey, R. Malloy, Q. Wang, J. Bokor, H. Dai, *Nano Lett.* **2003**, *4*, 123.
[18] A. M. Saleem, J. Berg, V. Desmaris, M. S. Kabir, *Nanotechnology* **2009**, *20*, 375302.
[19] J. Wang, G. Min, Z. Song, X. Ni, W. Zhou, J. Zhan, Y. Zhang, J. Zhang, L. Shi, *J. Mater. Chem.* **2012**, *22*, 21154.
[20] Z. Nie, E. Kumacheva, *Nat. Mater.* **2008**, *7*, 277.
[21] X. F. Zeng, S. C. Shei, S. J. Chang, *ECS Solid State Letters* **2012**, *1*, R27.
[22] C. Robert, A. C. Baratunde, F. Timothy, X. Xianfan, G. Ken, G. Samuel, *Nanotechnology* **2010**, *21*, 445705.
[23] J. Xu, T. S. Fisher, *Int. J. Heat Mass Trans.* **2006**, *49*, 1658.
[24] A. A. Balandin, *Nat. Mater.* **2011**, *10*, 569.
[25] X. Tian, M. E. Itkis, E. B. Bekyarova, R. C. Haddon, *Sci. Rep.* **2013**, *3*, 1710.
[26] C. L. Pint, N. W. Nicholas, S. Xu, Z. Sun, J. M. Tour, H. K. Schmidt, R. G. Gordon, R. H. Hauge, *Carbon* **2011**, *49*, 4890.
[27] G. Fiorentino, S. Vollebregt, F. D. Tichelaar, R. Ishihara, P. M. Sarro, *IEEE 27th International Conf. MEMS* **2014**, 342.
[28] D. N. Hutchison, N. B. Morrill, Q. Aten, B. W. Turner, B. D. Jensen, L. L. Howell, R. R. Vanfleet, R. C. Davis, *J. Microelectromech. Syst.* **2010**, *19*, 75.
[29] J. A. Weldon, B. Alemán, A. Sussman, W. Gannett, A. K. Zettl, *Nano Lett.* **2010**, *10*, 1728.
[30] P. M. Sousa, M. Gutierrez, E. Mendoza, A. Llobera, V. Chu, J. P. Conde, *Appl. Phys. Lett.* **2011**, *99*, 044104.
[31] V. Ivanov, J. B. Nagy, P. Lambin, A. Lucas, X. B. Zhang, X. F. Zhang, D. Bernaerts, G. Van Tendeloo, S. Amelinckx, J. Van Landuyt, *Chem. Phys. Lett.* **1994**, *223*, 329.
[32] S. Fan, M. G. Chapline, N. R. Franklin, T. W. Tombler, A. M. Cassell, H. Dai, *Science* **1999**, *283*, 512.
[33] T. Wang, K. Jeppson, J. Liu, *Carbon* **2010**, *48*, 3795.
[34] A. Misra, J. R. Greer, C. Daraio, *Adv. Mater.* **2009**, *21*, 334.
[35] A. Kis, G. Csanyi, J. P. Salvetat, T.-N. Lee, E. Couteau, A. J. Kulik, W. Benoit, J. Brugger, L. Forro, *Nat. Mater.* **2004**, *3*, 153.
[36] R. L. D. Whitby, W. K. Hsu, Y. Q. Zhu, H. W. Kroto, D. R. M. Walton, *Phil. Trans. R. Soc. Lond. A* **2004**, *362*, 2127.
[37] Y. Gogotsi, S. Welz, D. A. Ersoy, M. J. McNallan, *Nature* **2001**, *411*, 283.
[38] B. Morana, G. Pandraud, J. F. Creemer, P. M. Sarro, *Mater. Chem. Phys.* **2013**, *139*, 654.
[39] S. M. Spearing, *Acta Mater.* **2000**, *48*, 179.
[40] T. Taguchi, A. K. M. F. Kibria, S. Shamoto, *J. Phys.: Conf. Ser.* **2013**, *417*, 012037.
[41] R. Gupta, R. Mishra, K. Mukhopadhyay, R. Tiwari, A. Ranjan, A. Saxena, *Silicon* **2009**, *1*, 125.
[42] Z. Gu, Y. Yang, K. Li, X. Tao, G. Eres, J. Y. Howe, L. Zhang, X. Li, Z. Pan, *Carbon* **2011**, *49*, 2475.
[43] Y. Morisada, Y. Miyamoto, Y. Takaura, K. Hirota, N. Tamari, *Int. J. Refr. Metals Hard Mater.* **2007**, *25*, 322.
[44] J. Greer, D. Jang, X. W. Gu, *JOM* **2012**, *64*, 1241.
[45] T. Y. Lo, H. Z. Cui, H. C. Leung, *Mater. Lett.* **2004**, *58*, 2595.
[46] K. F. Chung, W. K. Yu, *Eng. Struct.* **2002**, *24*, 429.
[47] S. Pathak, E. J. Lim, P. Pour Shahid Saeed Abadi, S. Graham, B. A. Cola, J. R. Greer, *ACS Nano* **2012**, *6*, 2189.
[48] M. R. Maschmann, Q. Zhang, F. Du, L. Dai, J. Baur, *Carbon* **2011**, *49*, 386.
[49] C. San Marchi, A. Mortensen, *Acta Mater.* **2001**, *49*, 3959.
[50] P. B. Amama, C. L. Pint, S. M. Kim, L. McJilton, K. G. Eyink, E. A. Stach, R. H. Hauge, B. Maruyama, *ACS Nano* **2010**, *4*, 895.